THE PHOTOGRAMMETRIC RECORD

The Photogrammetric Record (2015)
DOI: 10.1111/phor.12099

APPLICATION OF ARCHIVAL AERIAL PHOTOGRAMMETRY TO QUANTIFY CLIMATE FORCING OF ALPINE LANDSCAPES

NATAN MICHELETTI (natan.micheletti@unil.ch)
STUART N. LANE (stuart.lane@unil.ch)
Institute of Earth Surface Dynamics, University of Lausanne, Switzerland

JIM H. CHANDLER (j.h.chandler@lboro.ac.uk)
School of Civil and Building Engineering, Loughborough University, UK

Abstract

Recent and future climate change may lead to landscape changes in geomorphic processes and process rates. Such modifications are likely to be widely distributed, making their direct measurement difficult and there are almost no such measurements at decadal intervals. Aerial imagery has been acquired by many national agencies since the 1950s and significant archives remain. Unlocking the information from these data sources is important because their timescale may inform significant unresolved hypotheses regarding the impact of rapid climate change on Alpine environments. However, such photogrammetric applications are challenging because of topographic complexity (including occlusions and large elevation ranges) and variations in image texture. A complete workflow is described from raw data to the treatment and interpretation of results. This is applied to imagery of Val d'Héréns, Switzerland, a landscape containing an assemblage of glacial, periglacial, hillslope and fluvial landforms across a height range of 1800 to 3600 m from the 1960s to the present. These changes reveal important characteristics of landscape scale erosion and deposition at the decadal scale.

KEYWORDS: aerial photogrammetry, archival imagery, climate forcing, digital elevation model, geomorphic changes, geomorphology

INTRODUCTION

GEOMORPHOLOGICAL RESEARCH IS ALWAYS in need of three-dimensional data to describe topographic surfaces and to monitor their change over time. The possibility of generating quantitative elevation data from stereo photography has played an important role in this regard, as demonstrated by pioneer applications of photogrammetry to geomorphological studies (Wickens and Barton, 1971; Welch and Jordan, 1983; Small et al., 1984; Chandler and Cooper, 1988; Chandler and Moore, 1989; Lane et al., 1994). With the advent of fully

automated methods and the transition from traditional to digital photogrammetry during the 1990s, photogrammetry became a widely used, cost- and time-effective approach for geoscience research (Lane et al., 2000). Crucially, it represents a unique resource for deriving three-dimensional data of past landscapes using the extensive coverage of aerial imagery commonly available since the 1950s. This type of application, named archival aerial digital photogrammetry, has proved successful for a wide range of fields, including fluvial geomorphology (Lane et al., 2003; 2010), permafrost and periglacial processes (Kääb and Vollmer, 2000; Kneisel and Kääb, 2007; Fischer et al., 2011), and hillslope processes (Chandler and Brunsden, 1995; Walstra et al., 2007; Schwab et al., 2008; Bennett et al., 2013).

Despite the ease with which elevation data can be extracted from imagery, including new photogrammetric methods like structure from motion (SfM) (for example, Fonstad et al., 2013), the application of digital photogrammetry for geomorphological research still poses the following complications:

(1) The ease of automated data generation offered by digital photogrammetry may cause the user to underestimate data quality issues (Cooper, 1998; Lane et al., 2000) or to overlook key data quality controls (James and Robson, 2014). This is problematic because in spite of the advanced algorithms and automated processes offered by digital and emerging forms of photogrammetry, conventional controls upon photogrammetrically derived data are still crucial and need careful consideration.
(2) The application of aerial digital photogrammetry in areas of complex or rough topography and large elevation ranges can be problematic, particularly occlusions caused by sudden elevation changes or where the density of the acquired data is low in areas of complex topography.
(3) Because archival aerial imagery may have been acquired at a large range of flying heights, its scale may be unsuitable for generating precise elevation data within small areas. Accordingly, the limits of detectable changes need to be carefully considered to ensure correct interpretation of results.
(4) Older aerial photographs can be characterised by imagery of low contrast and varying quality, which improved with time as photogrammetric emulsions evolved; data processing and the quality of final results will inevitably be affected by this variability.

Sediment production and transfer together with glacial and periglacial processes in high mountain basins are potentially sensitive to the significant changes in climatic conditions that have affected the European Alps over the past century. Understanding the effects of such changing conditions upon landscapes is challenging because of the difficulty of investigating this climate forcing (the difference in insolation (sunlight) absorbed by the earth and energy radiated back into space) over decades to centuries, despite this being the timescale over which significant hypotheses are raised over human impacts upon climate change and consequently geomorphic systems (Reynard et al., 2012; Knight and Harrison, 2013). Archival aerial imagery offers a unique opportunity to address this scientific topic (Schwab et al., 2008; Bennett et al., 2013). The research described in this paper seeks to describe the complete workflow adopted for the application of archival aerial photogrammetry in the Swiss Alps to assess the extent to which geomorphological changes associated with climate forcing can be quantified in high mountain landscapes.

A sequence of aerial imagery from the 1960s to the present day has been used to compute digital elevation models for Val d'Héréns, Switzerland (Fig. 1). The case study

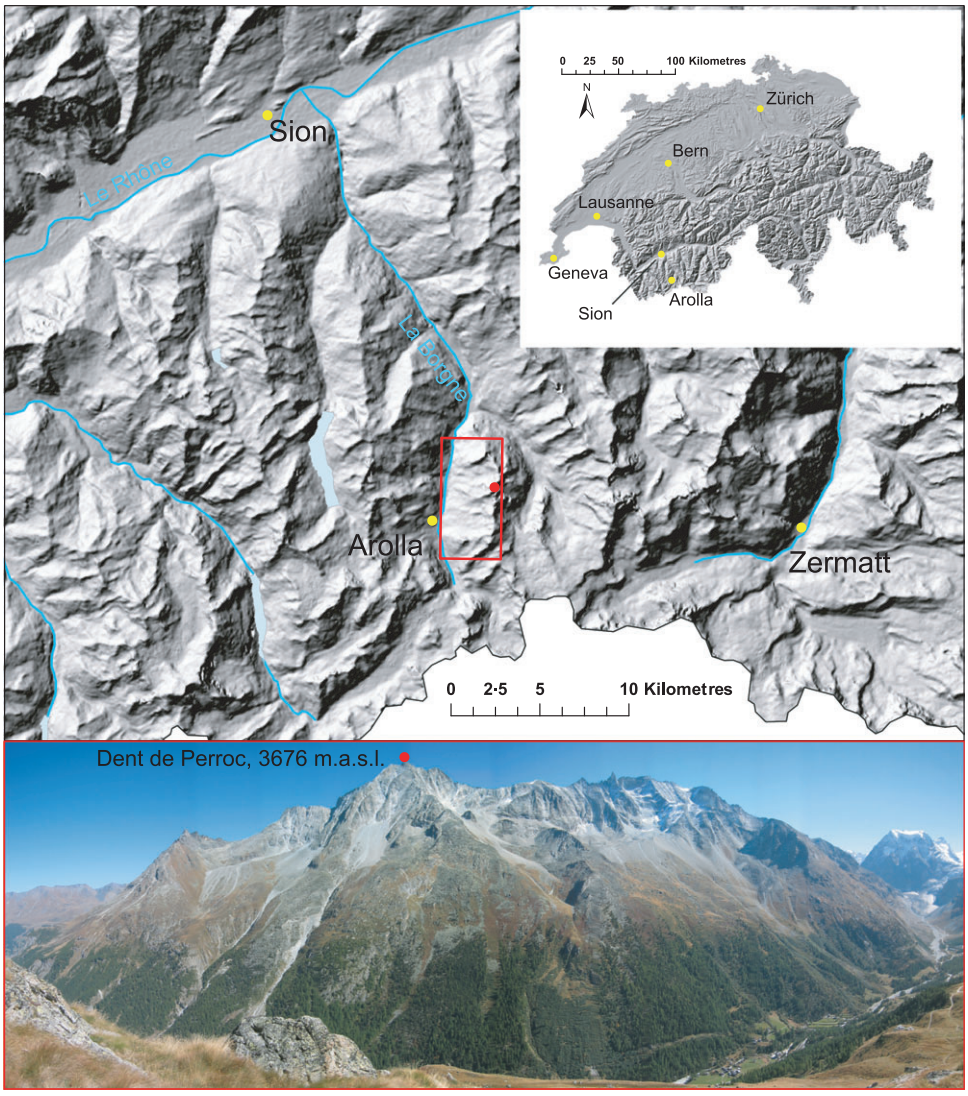

FIG. 1. Case study area near Arolla, Héréns Valley, Switzerland, indicated by the red rectangle. The peak of Dent de Perroc is indicated by the red dot on both the map and photograph. Relief shading and river data: Swisstopo. Photography by C. Lambiel, 2004.

consists of a steep deglaciated zone, ranging from about 1800 to 3600 m above mean sea level (a.s.l.). The area is comprised of an actively changing, and hence locally dynamic, assemblage of glacial, periglacial, hillslope and fluvial landforms. It is likely to be sensitive to climate forcing, by virtue of landforms highly sensitive to temperature changes (glaciers and permafrost) and because of the presence of unconsolidated, historically weathered and glacially derived material, representing high potential for significant sediment mobilisation.

In presenting the workflow, the issues that arise at different stages of the data processing are identified and solutions are proposed which are applicable even with limited ground control data. Thus, guidance, advice and caveats are offered for the potential geomorphological applications of archival aerial photogrammetry in high mountain environments. All photogrammetric data processing has been performed using ERDAS IMAGINE Leica Photogrammetry Suite (LPS) 2010, released in November 2009, while post-processing operations and results analysis have been implemented using Matlab and ArcGIS.

AERIAL IMAGERY AND INTERIOR ORIENTATION

The archival aerial images used in the study were acquired by the Swiss Federal Office of Topography (Swisstopo) using a range of different analogue cameras. These include a number of 23 cm × 23 cm images for seven distinct epochs, all collected at similar periods of the year (end of summer–beginning of autumn) with flying heights varying between 5000 and 7000 m a.s.l. These have been scanned by Swisstopo at a resolution of 14 μm (1814 dpi) using a photogrammetric-quality scanner and vary in scale between 1:15 700 and 1:28 000. The fore-and-aft (forward) overlap between two consecutive frames in a flight line is about 80%, which is a routine Swisstopo policy because of the high relief displacement in such mountainous areas.

An eighth set of aerial photographs was acquired in 2012 by Flotron using an UltraCam-X digital camera, which represents the most recent dataset of the study. The UltraCam-X camera is equipped with four panchromatic and four multispectral lenses. The images are composed of 14 430 × 9420 pixels of 7·2 μm (about 10·39 cm × 6·78 cm frame size) and have a scale of 1:5200. The lateral overlap (sidelap) specification was also 80%; therefore, 12 images were used to cover the whole area of interest. The list of images used for the study and their characteristics are presented in Table I.

A block file representing each epoch was created in ERDAS LPS, using either frame or digital camera geometric models for Swisstopo and Flotron imagery, respectively, and employing the Swiss coordinate system with the geodetic datum CH1903. Calibration

TABLE I. Characteristics of the aerial imagery available from Swisstopo and Flotron in 2012.

Date	*Scale*	*Lens type*	*Emulsion*	*Calibrated focal length (mm)*
(1) 28th September 1967	1:15 700	Leica 15 UAG 120	BW	152·87
(2) 8th September 1977	1:20 900	Leica 3008 15 UAG II	BW	153·02
(3) 19th July 1983	1:19 000	Leica 15/4 UAG	BW	153·37
(3) 7th September 1983	1:20 900	Leica 15/4 UAG	BW	153·37
(4) 10th August 1988	1:20 900	Leica 15/4 UAG	BW	153·37
(4) 10th August 1988	1:23 500	Leica 15/4 UAG	BW	153·37
(5) 7th October 1995	1:26 800	Leica 15/4 UAG-S	BW	152·52
(6) 2nd September 1999	1:26 000	Leica 15/4 UAG-S	RGB	152·52
(6) 2nd September 1999	1:28 000	Leica 15/4 UAG-S	RGB	152·52
(7) 17th August 2005	1:24 600	Leica 15/4 UAG-S	RGB	153·51
(7) 17th August 2005	1:24 800	Leica 15/4 UAG-S	RGB	153·51
(8) 20th September 2012	1:5200	UltraCam-X lenses (4 PAN; 4 MS)	RGB-NIR	100·50

BW = black and white; RGB = red, green, blue (colour); NIR = near infrared; PAN = panchromatic; MS = multispectral.

certificates were available at www.swisstopo.admin.ch. This resource provided: (a) the calibrated focal length (principal distance); (b) radial distortions referenced to the principal point of symmetry (PPS); (c) PPS displacement with respect to the focal centre (FC); and (d) fiducial mark coordinates referred to the FC. To complete the definition of the internal geometry of the camera, the fiducial marks were manually measured on the images and a 2D affine transformation established to determine the origin of the photo coordinate system (Intergraph Corporation, 2014). This transformation was achieved with a sub-pixel root mean square error (RMSE), typical for this type of imagery.

The Flotron digital imagery was provided with a calibration file for the digital camera. This provided the calibrated focal length (100·50 mm) and the PPS offsets. Imagery was corrected by Flotron to show no significant radial distortions. Calibrated fiducial marks and associated management were not necessary because the photo coordinate system can be defined simply by indicating the pixel dimensions (7·2 μm × 7·2 μm) in ERDAS LPS.

Field Data and Exterior Orientation

Considerable fieldwork was required to establish an appropriate number of ground control points (GCPs) necessary for photogrammetric restitution where the unstable high mountain environment creates significant challenges. The GCPs need to satisfy two requirements: (a) stable over time (that is, not moving or changing in appearance during the period of study); and (b) easily and precisely identifiable on the images. Finding sufficient points with these characteristics can be problematic in an active landscape where some areas are typically: (a) difficult to access; (b) may or may not be experiencing movement over a 50-year period; and (c) may be devoid of infrastructure. Ideal candidates for this kind of study are the corners of roofs of traditional and un-renovated buildings, but use had to be made of the centre of isolated, medium-sized, round-shaped boulders (approximately 2 m in diameter was appropriate given the scale and resolution of the imagery) located in clearly stable areas. Such boulders were preferred because they can be easily identified on images and the uncertainty when measuring their apparent centre is limited. It is also fundamental that the points provide adequate coverage across the site, including a wide elevation range.

Two Leica System 500 differential global positioning system (DGPS) units were used to obtain the required control for the case study, the field campaign being carried out in July 2012. A total of 169 GCPs were measured along the valley bottom and mountainsides, across an area of approximately 20 km^2 (3 km × 6·5 km) and with an elevation range of more than 1000 m (1808 to 2828 m a.s.l.) (Fig. 2). A DGPS base station was established early in the field programme and 6 h of static observations obtained. Data were subsequently downloaded from the nearest available Automated GNSS Network for Switzerland (AGNES) located in Martigny, 30 km away in the Rhône valley. These were post-processed in Leica Geo Office to correct coordinates to the Swiss national coordinate system CH1903. Visual inspection of the horizontal displacements derived by the correction using Swisstopo orthophotos is shown in Fig. 3. It was not possible to survey all the points using a single base station because of limitations in radio communication, either because of the base-to-rover distance or due to topographic screening. Three further base stations were established in the valley, all linked directly to the initial base station. Subsequent post-processing of the original real time kinematic (RTK) data allowed the determination of the coordinates of all GCPs in the CH1903 system. All GCP coordinates were estimated with a precision better than ±0·05 m.

To estimate initial exterior orientation parameters associated with each image, the GCPs were manually measured and assigned to the corresponding point on the images. It

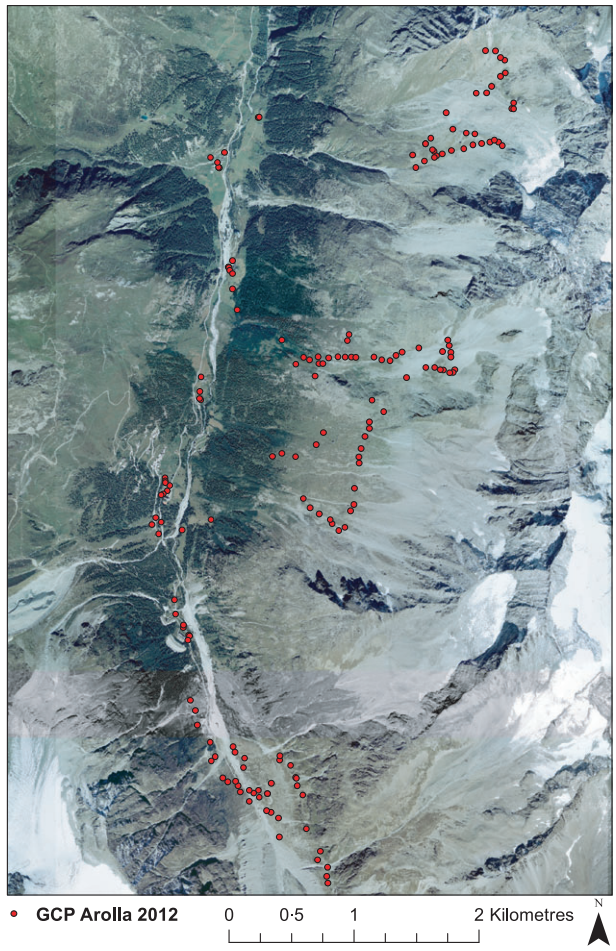

FIG. 2. Ground control point distribution in the Arolla Valley, Switzerland, shown by red dots.

was not necessary to measure all GCPs, and neither could every GCP be found or identified precisely. The availability of a large dataset of GCPs reduced the reliance upon individually measured points, hence improving the quality of the solution. After having identified a sufficient number of control points, well distributed in space and with a large elevation range, a proportion were reclassified as check points. Check points are not used to estimate the exterior orientation parameters but to provide a direct estimate of the accuracy of the restitution. This is done in terms of discrepancy between the photogrammetrically derived position and the GCP coordinates.

After solving the initial bundle adjustment using just GCP measurements, it was possible to perform automatic tie-point extraction. However, and as mentioned in similar studies (for example, Fischer et al., 2011), this procedure is not efficient for areas including extremely steep terrain and exhibiting many shadows. Therefore, either automatically generated tie points needed to be checked manually or the tie points should be measured

FIG. 3. Ground control points before (red) and after (green) applying the post-processing correction using Swiss Automated GNSS Network data. The point, located in a stable area near a path, was measured at the centre of the boulder, but it was necessary to correct the newly established DGPS base position to derive correct coordinates.

manually. An additional problem arose during the processing of the Flotron 2012 imagery. GCPs could not be surveyed on all parts of the mountainside because of dangerous and difficult access in regions of cliffs. This was problematic since, given the large scale of the 2012 images, there were an insufficient number of control points for some frames and LPS (and traditional photogrammetric packages) requires a sufficient number of GCPs for successful solution of the bundle adjustment. To address this issue, a well-established GCP transfer procedure was adopted (see Lane et al., 2010). First, a bundle adjustment was obtained for those images where sufficient GCPs were available. Second, on these images, clearly identifiable features were found and marked as common tie points where they were also visible on images without sufficient GCPs. Third, these tie points were relabelled as GCPs and were measured on the images without sufficient GCPs; the measurements were used to obtain a bundle adjustment for all of the imagery. As explained in Lane et al. (2010), it is important to note that these new GCPs have a poorer precision than those surveyed directly in the field using DGPS. However, this approach provided a viable and satisfying solution for images with insufficient GCPs.

ERDAS LPS uses a conventional bundle adjustment to perform the aerial triangulation and to estimate exterior orientation parameters for each image used (Intergraph Corporation, 2014). In this procedure, image point and GCP standard deviations are crucial and need to be commensurate with the expected precision of both image measurements and object control. This allows for more flexibility during the bundle adjustment and leads to a better solution. Image point standard deviations can be indicated in pixel units and should be related to the measurement precision and image quality/resolution. These values were changed to 0·5 for the scanned Swisstopo imagery, whilst the default value of 0·3 was used for the digital Flotron 2012 imagery. GCPs were constrained to an object precision of 0·5 m in plan and 0·3 m in height. These globally applied values were chosen to account for the following uncertainty sources: (a) imprecision in measuring the centres of boulders or in

surveying non-horizontal boulders in steep zones; and (b) uncertainty in DGPS measurements themselves, including post-processing with AGNES data.

ERDAS LPS offers a number of indicators to estimate the quality of the exterior orientation solution. The total image unit-weight (TIUW) RMSE is a global precision indicator describing the quality of the entire solution in the image space (Intergraph Corporation, 2014). Root mean square errors for both control and check points are also provided, and for both ground coordinates (X, Y, Z) and stereo intersection accuracy in image coordinates (x, y) (Fischer et al., 2011; Intergraph Corporation, 2014). The aerial triangulation summary for each epoch is presented in Table II. Overall, the bundle adjustment yielded very satisfying results and in accordance with what was expected assuming the known data quality. This is of fundamental importance because it has been shown that random error in a bundle adjustment can translate into systematic error in the stereomatching derived data (for example, Lane et al., 2004), and so effort is required to minimise them. These data also give a preliminary indication of the possible precision of data points extracted from the imagery although, as discussed below, this may be downgraded according to the success of the stereomatching process.

AUTOMATIC STEREOMATCHING

In digital photogrammetry, automatic stereomatching algorithms are used to identify homologous point pairs and to compute their ground coordinates using exterior orientation parameters (Dissart and Jamet, 1995). These algorithms are based upon detecting similar image intensity patterns within either small image "areas" or located around distinct "features". This distinction is the basis of classifying the approaches into either feature-based or area-based (Remondino et al., 2014). Feature-based approaches achieve correspondence between interest points. These are locations which exhibit "distinctness" and identified using an interest operator, generally attributed to Förstner (1986). On the other hand, area-based methods correlate small windows of pixels on two images to perform the matching. Accordingly, crucial to the matching process is sufficient texture or variations in pixel intensity in the images (Lane et al., 2000; Remondino et al., 2014). In ERDAS LPS, two area-based stereomatching algorithms are now available, Automated Terrain Extraction (ATE) and enhanced Automated Terrain Extraction (eATE), the latter being capable of classifying points. Both eATE and ATE were evaluated and considered but ATE required more modest computing resources and was more rapid, easier to use and hence more

TABLE II. Exterior orientation performances.

Year	*TIUW*	*Control point RMSE*					*Check point RMSE*				
	RMSE	*X*	*Y*	*Z*	*x*	*y*	*X*	*Y*	*Z*	*x*	*y*
1967	0·41	0·46	0·43	0·15	0·31	0·31	0·42	0·23	0·26	0·07	0·11
1977	0·30	0·28	0·28	0·14	0·29	0·30	0·41	0·07	0·18	0·32	0·01
1983 (July)	0·32	0·23	0·29	0·14	0·41	0·33	0·15	0·45	0·44	0·24	0·09
1983 (Sept)	0·31	0·30	0·27	0·10	0·29	0·30	0·45	0·15	0·43	0·21	0·08
1988	0·33	0·41	0·45	0·26	0·44	0·35	0·36	0·30	0·45	0·21	0·39
1995	0·29	0·29	0·37	0·19	0·32	0·25	0·09	0·29	0·56	0·28	0·18
1999	0·36	0·30	0·31	0·22	0·35	0·30	0·38	0·33	0·38	0·25	0·20
2005	0·34	0·22	0·28	0·17	0·28	0·33	0·25	0·27	0·38	0·26	0·21
2012	0·17	0·12	0·13	0·14	0·17	0·19	0·28	0·24	0·18	0·14	0·22

TIUW = total image unit-weight; X, Y, Z ground coordinates are in metres; x, y photo coordinates are in pixels.

effective. In addition, ATE has been successfully used in the past on a range of projects (Walstra et al., 2007; Lane et al., 2010) and was therefore adopted for this study. ATE exploits the epipolar constraint to improve the image-matching process and offers customisable strategy parameters for optimising results, along with suggested parameter sets for a number of terrain types (such as high mountains, rolling hills, urban areas and so on). These parameters may strongly influence coordinate determination in mountainous regions (Lane et al., 2000). Among the parameters available, the correlation coefficient limit, the correlation window size and the search window size on the epipolar line are indicated as the most important (Leica Geosystems Geospatial Imaging, 2006). The correlation coefficient limit indicates the minimum acceptable correlation for two matched pixels for the point to be accepted. A high coefficient threshold inevitably identifies only high-quality matches (Lane et al., 2000). It is obvious that a trade-off is necessary for this parameter; keeping only high-quality matched points means that the total number matched is smaller, which can be a problem in mountainous topography where the relief can be complex. On the other hand, accepting low-correlation matches can allow false matches to be included in the dataset and hence produce poorer quality data. The default value for this parameter for high mountains is 0·8 (Intergraph Corporation, 2014). The correlation window size is the size (in pixels) of the area used for computing the correlation coefficient between sets of pixels on different images. This usually needs to be smaller for areas containing large variations in topographic relief, grey level or colour intensity; the default value proposed by ERDAS LPS (Intergraph Corporation, 2014) for high mountain regions is 7×7 pixels. The search window size across the epipolar line can be adapted to help point matching in cases where the exterior orientation is of low quality; that is, to permit the matching of points further away from the epipolar line. Finally, the user needs to indicate the output cell size, which determines the resolution of the rasterised digital elevation model (DEM). In this research, for reasons explained below, point clouds of ground coordinates generated from matched points and exterior orientation parameters are preferred as output instead of an already rasterised or triangulated DEM.

The strategy parameters would be expected to affect different surface characteristics in different ways, not least because surface cover influences image texture. Thus, to assess strategy parameter effects, a very high density of check data is needed, and certainly beyond what could be acquired practicably during a normal field campaign (Lane et al., 2004). The alternative is to use sensitivity analysis where key parameters are varied one at a time to quantify their effects on estimated elevations (for example, Lane et al., 2000; Gooch and Chandler, 2001). Consequently, the effect of varying the correlation coefficient limits (from 0·7 to 0·9) and correlation window sizes (from 5×5 to 11×11 pixels) was quantified. The comparison of results is performed at the level of point clouds (X, Y, Z coordinates), by associating points within a Euclidean distance of 0·5 m in X and Y, and comparing their elevation in order to assess the sensitivity of the extracted data to strategy parameters. For this detailed sensitivity analysis, two pairs of images from the 1988 epoch were used. Three regions of interest (ROIs) with contrasting terrain characteristics and image texture were identified for the analysis (Fig. 4(a)): (a) a field of large boulders; (b) a zone of fine sediments and texture; and (c) a steep area with abrupt elevation changes. Changing the correlation window or the search window sizes did not produce any change for any of the three ROIs, an outcome that can be explained by the robustness of the exterior orientation solution and the presence of sufficient texture in the images. However, modifying the correlation coefficient limit has important consequences. Increasing the coefficient from 0·7 to 0·8 causes a reduction of about 10% in the number of extracted points, while an increase from 0·8 to 0·9 only produces a further 3% reduction. This is satisfying since it indicates

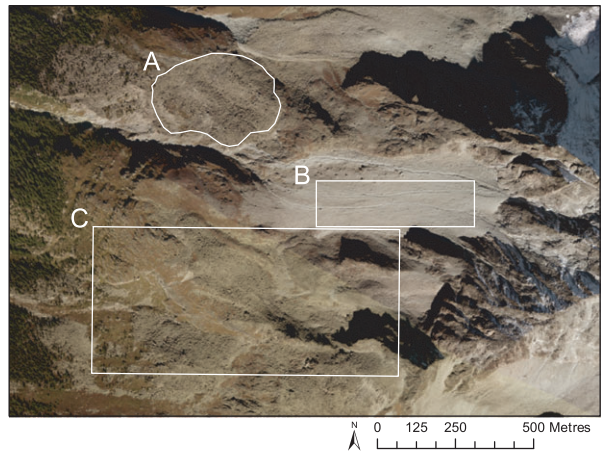

(a)

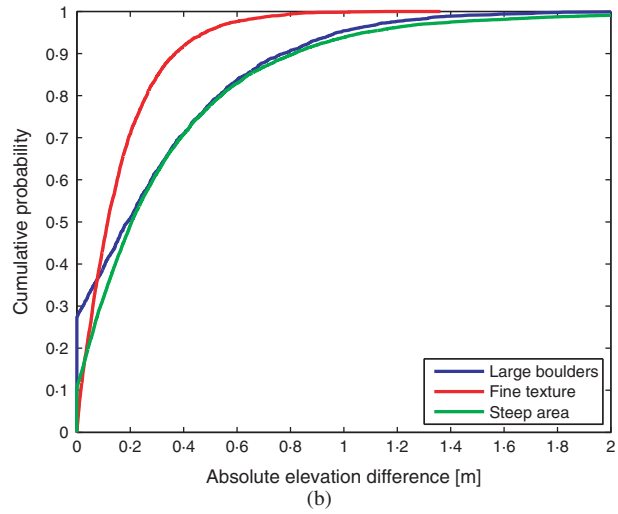

(b)

FIG. 4. (a) Zones of different morphology and texture (A, large boulders; B, fine texture; C, steep area). (b) Effect of correlation coefficient parameter change (from 0·8 to 0·9) on single points for zones of different morphology and texture shown in (a).

that using the suggested value for high mountain environments (0·8) provides good-quality output. Furthermore, changing the correlation coefficient also causes elevation changes to some points (Table III). These differences have an expectation μ and a median Q_{50} of zero for each ROI, although, the degree of spread varies. To help interpret the distribution of elevation differences, the cumulated distribution of the absolute elevation discrepancies is shown in Fig. 4(b). The latter demonstrate that the majority of points are not sensitive to the strategy parameters, as confirmed by the low value containing two-thirds of absolute residuals (the 66% quantile (0.66) in Fig. 4(b) corresponding to 0·17 m elevation difference for the fine texture zone and 0·34 m for the other two).

TABLE III. Distribution statistics of elevation difference caused by changing the correlation coefficient parameter from 0·8 to 0·9 on single points.

Zone	μ	σ	Q_{50}	$\mu(abs(\mathrm{d}Z))$	Q_{50} *of abs*	Q_{66} *of abs*
Boulders	0	0·45	0	0·29	0·19	0·34
Fine texture	0	0·23	0	0·16	0·12	0·17
Steep area	0	0·62	0	0·34	0·20	0·34

μ is the expectation; σ is the standard deviation; Q_{50} *of abs* is the median and Q_{66} *of abs* the 66% quantile of the absolute height differences *abs*(d*Z*).

Changes in stereomatching strategies appear to affect only some points in the generated DEM. This justified further use of the failure warning model (FWM) developed by Gooch and Chandler (2001), who employed it to demonstrate that changing strategy parameters affect only less robust points in steep, low-texture or shadowed areas, whilst elevation estimations for the remainder of the derived points are almost unaffected. In this study, FWM was used as an informative tool to define automatically areas that are susceptible to changes in the strategy parameters and thus where elevation data are unreliable. This approach is used to justify the use of the strategy parameters employed and provides an alternative to the lengthy and demanding parameter optimisation process, which requires independent data.

The principle of the FWM is that the sensitivity of strategy parameters can be used to identify areas where elevation data quality is likely to be poorer and thus provide a caveat for further DEM use. The FWM algorithm includes two parts:

(1) The slope in an area around interpolated points is investigated to identify unreliable interpolation estimates, which is particularly critical in complex or steep topographic zones.
(2) The identification of areas susceptible to changes in the strategy parameters using DEMs of difference (DoD). In this stage, the value of each point in the difference image is examined individually. If that value is greater than the standard deviation σ of all points in the model multiplied by a user definable parameter A (here $A = 1$), the point is tagged as sensitive:

$$\left|\mathrm{DoD}_{x,y}\right| > A \cdot \sigma(\mathrm{DoD}).$$

To continue the investigation of the effect of varying the strategy parameters on the stereomatching procedure, phase (2) of the FWM was applied here for the 1959 and 1988 epochs (Fig. 5). Results are consistent between the two years, with similar zones sensitive to strategy parameters highlighted by the model. These correspond mostly to steep, low-texture or shadowed areas. In contrast, the rest of the area does not seem to be affected by changes in the strategy parameters. On this basis, the final data were processed using the suggested parameters for high mountain areas for every epoch, and the observation regarding the lower confidence of data points in relatively steep, low-texture or shadowed areas was noted. A masking procedure is necessary to address issues in these areas, as explained later.

DATA POST-PROCESSING

For each image used in this research, raw point clouds of ground coordinates generated from matched points were extracted using the ATE DEM extraction module in LPS. Despite

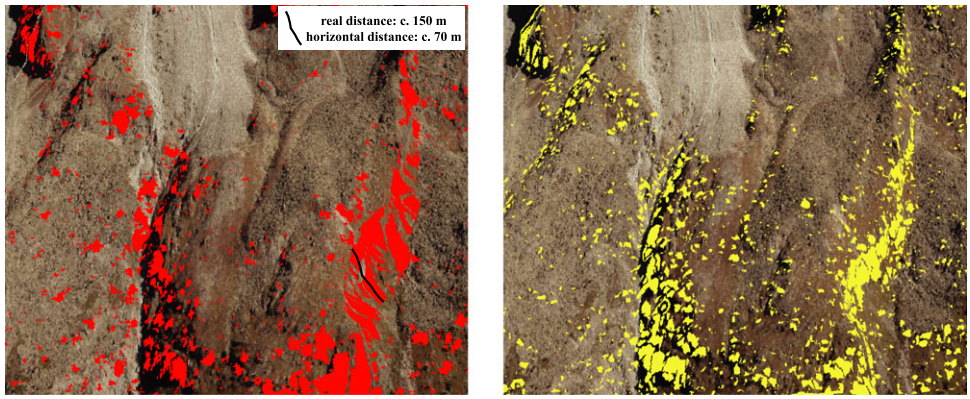

(a) 1988 (b) 1959

FIG. 5. Example of 3D visualisation of failure warming model (FWM) output for: (a) 1988 (red); and (b) 1959 (yellow) imagery, generating similar results in highlighting very steep or low-textured areas.

a robust bundle adjustment and stereomatching parameters adapted to mountain regions, the derived elevation data can still present errors in the form of mismatched points that generate either negative or positive spikes. A common practice to address these issues is the application of a filter over the rasterised DEM, typically a low-pass filter, but this is known to cause loss of detail and possible propagation of error into good points (Lane et al., 2004; Milledge et al., 2009). Hence, it is preferred to adopt an approach able to identify and remove elevations that are probably incorrect. To perform this operation, the following two filtering methods were adopted:

(1) The first employs a statistical Chauvenet-type criterion using reliable external elevation data in the form of a coarse registration DEM (25 m resolution Swisstopo DEM from 2005). Each derived elevation Z_p is evaluated as follows:

$$|Z_p - Z_c| > 1.96\ stdfilt\ (coarse\ DEM)$$

where Z_p is the elevation of a stereomatching derived point, Z_c is the pixel value of the coarse DEM where the point falls and *stdfilt (coarse DEM)* is the standard deviation of the elevation in the 3×3 neighbourhood around this pixel. This condition identifies elevations that significantly differ from the coarse DEM. By using a locally derived standard deviation, the algorithm allows for large differences in steep zones but is less permissive in flatter areas. Since it relied on a 2005 DEM in this study, it is clear that the filter is not reliable where local rates of elevation change over time are high. Therefore, a geomorphological map (Lambiel et al., 2015) was used to identify zones matching this condition, such as glaciers, debris-covered glaciers, push moraines or rock glaciers. The filter was not applied in such regions.

(2) The second method is a topographic criterion using localised slope data to detect spikes. A triangulated irregular network (TIN) was generated from the point cloud and slopes steeper than 50° were highlighted. Points responsible for these slopes were removed and the TIN updated to deal with clusters of erroneous points. The iteration was completed three times. This method is clearly not reliable for very steep slope zones or cliffs, hence these areas were identified and removed from the analysis.

The combined outcome for both methods was used to decide whether to retain or remove points, and the geomorphological map (Lambiel et al., 2015) was employed to use the filter more appropriately to the local land surface. DEM error is supposed to vary with the type of surface and hence error-handling procedures should be sensitive to surface type and be adaptable to ensure retention of good-quality points. Further, this procedure was applied only in cases where the derived data seemed to contain erroneous points in order to avoid the unnecessary elimination of high-quality points.

An interpolation in the geographical information system (GIS) environment ArcGIS was performed to generate the final 1 m resolution raster DEMs using ordinary kriging, with polynomial trend removal of order 3 and a stable variogram model. Since the derived datasets generally have a high density of points, the effect of the interpolation on the result is expected to be considerably reduced. However, areas with lower densities are indeed present and are very sensitive to the choice of the interpolator and its parameters. In this regard, comparative analysis of interpolators is discussed in the literature such as Aguilar et al. (2005) and Arun (2013). Where more than one image pair was necessary to cover the ROI, mosaicking was performed in ERDAS 2010 using the overlapping function "feather". Examples of hill shading for 2012 data and for archival Swisstopo imagery are presented in Fig. 6.

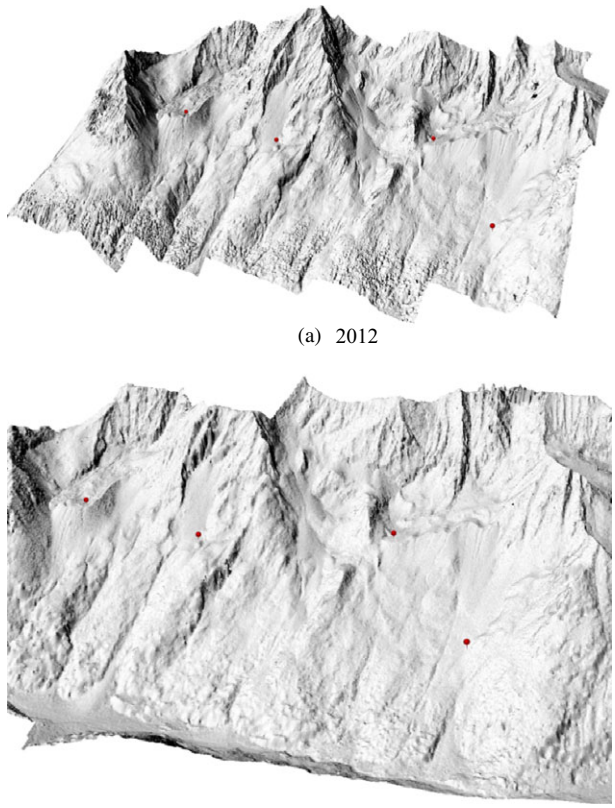

(a) 2012

(b) 1988

FIG. 6. Examples of hill shading with examples of four common points in red: (a) recent Flotron imagery from 2012; (b) archival Swisstopo data from 1988.

QUALITY ASSESSMENT AND ERROR PROPAGATION

The final DEMs should be evaluated to establish their quality. This may be achieved by taking datasets from different dates and comparing individual data points for zones where it is absolutely certain that no changes have occurred (Dewez et al., 2013). In this research it could not be assumed that there were zones of no change and so it was necessary to focus upon high-resolution and high-quality independent data points. However, such data are not typically available in this kind of study and, therefore, it can be challenging to obtain a reliable estimation of the quality of a derived DEM. In this case there were a number of high-quality spot measurements in the form of unused GCPs, and these were available for quality assessment. In this analysis, only points on the hillslope were used to assess the final DEMs. As in Lane et al. (2000), the error was defined as the difference in elevation between the DGPS measurement and the DEM value at that location, and the error value is used to compute accuracy in the form of the mean error (ME) and precision in the form of the standard deviation of error (STD) as follows:

$$\mathrm{STD} = \sqrt{\frac{\sum_{i=1}^{n}((p_i - s_i) - (\overline{p_i - s_i}))^2}{n}}$$

where p_i and s_i are the associated photogrammetric DEM and DGPS survey elevations, respectively. Use of the ME and the STD in this way requires the errors to be Gaussian, which is often not the case in digital photogrammetric applications (Höhle and Höhle, 2009). Gaussian error allows a probabilistic confidence approach to the propagation of error (see below). If the errors are not Gaussian, alternative approaches are needed to estimate random error. Höhle and Höhle (2009) proposed guidelines for robust accuracy measures suited to a non-normal error distribution based on quantile descriptors.

To investigate the normality of the error distribution, measured quantiles (Q) were plotted against the quantiles of a normal distribution having the same mean and standard deviation, in a Q–Q plot, and the two cumulative distribution functions were compared (Fig. 7). Additionally, the Lillifors test was used to evaluate the null hypothesis that DEM errors are normally distributed. In every case the hypothesis was accepted at the 5% significance level. The outcome verified that all DEM error distributions follow a normal distribution.

Table IV summarises the quality of DEMs for each year. The MEs are not null, indicating a small bias in the DEMs. Effectively, DGPS elevations are generally higher than their DEM equivalents and there is no spatial structure in this bias. To provide a better estimation of absolute elevation changes between the years, these biases have been removed by adding the ME to each DEM.

This study is concerned with quantifying climate forcing of Alpine landscapes, that is, investigating the possible link between climatic conditions and morphological changes in the landscape. The identification of patterns of erosion and deposition from DoD is a fundamental aspect in this regard. Moreover, it is necessary to adopt a framework to quantify the confidence that apparent erosion and deposition patterns are real changes and not noise associated with random errors in surfaces computed using digital photogrammetry. On the basis of the framework for error analysis proposed by Taylor (1997), Lane et al. (2003) applied an error propagation methodology where the uncertainty in the magnitude of

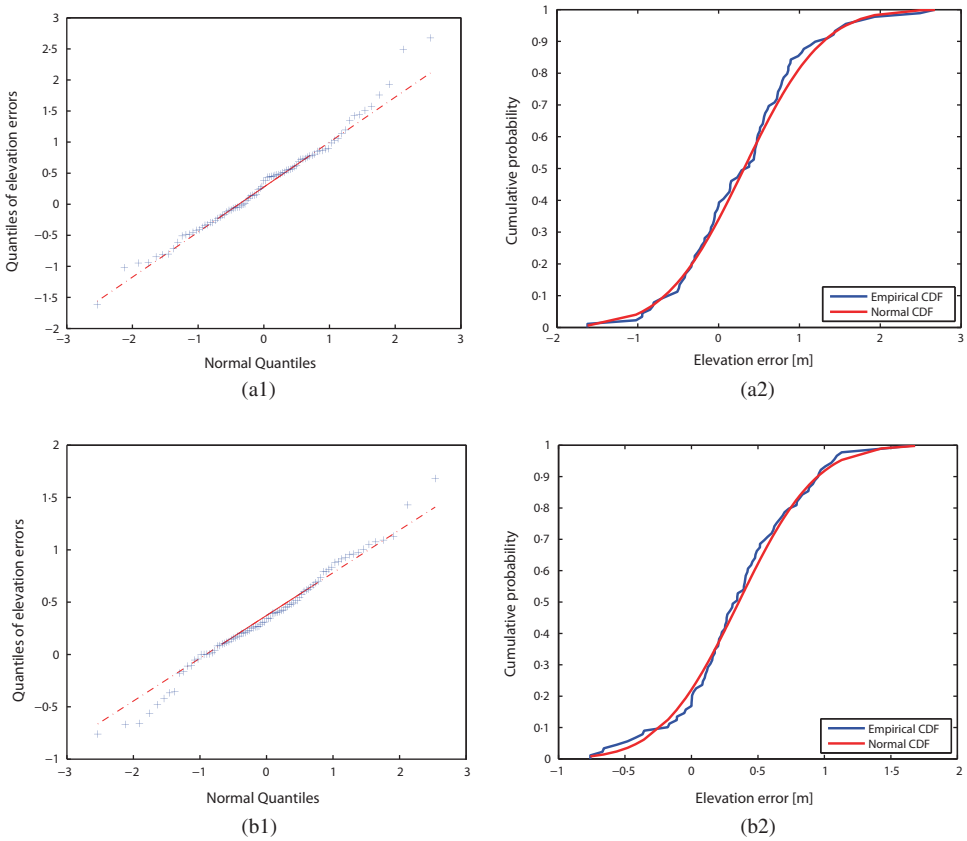

FIG. 7. Q–Q plot (left - 1) and cumulative distribution function (right - 2) of error data versus a standard normal distribution: (a) oldest (1967) DEM; (b) most recent (2012) DEM.

TABLE IV. DEM precision and accuracy assessment using DGPS survey data.

DEM date	*1967*	*1977*	*1983*	*1988*	*1995*	*1999*	*2005*	*2012*
ME	0·315	0·504	0·281	0·296	0·541	0·493	0·453	0·356
STD	0·765	0·820	0·953	0·644	0·751	0·827	0·998	0·462

ME = mean error; STD = standard deviation of error.

change σ_c in the DoD is determined by the root of the sum in quadrature of the uncertainties σ_1 and σ_2 associated with the two individual DEMs:

$$\sigma_c = \sqrt{\sigma_1^2 + \sigma_2^2}.$$

The STD is used here as a measure of uncertainty, but it can be employed to formulate statistical testing of the significance of each elevation difference $Z_1 - Z_2$ using a t test (Lane et al., 2003):

$$t = \frac{Z_1 - Z_2}{\sqrt{\sigma_1^2 + \sigma_2^2}}.$$

This equation can be used to threshold the DoD, hence labelling elevation differences within the threshold as noise. With $t = 1$, the confidence limit for detection of change is 68%. In the research described here, the minimum level of detection was set with a confidence limit of 90% ($t = 1{\cdot}64$). This was selected to have greater confidence that a discrepancy is indeed significant and represents real geomorphological change, whilst maintaining enough informative signals in the DoD. Table V summarises the limit of detection of change (LDC) at this confidence limit for DoDs computed between different epochs. The change detection that can be achieved corresponds to ± 1 to ± 3 parts per 10 000 of the flying height.

The last operation that was necessary prior to DoD analysis required an irresolvable aerial photogrammetric issue to be addressed: DEM comparisons in near-vertical rockwalls or forested areas. Steep rock faces and trees can create significant occlusions because of the differences in position of the cameras associated with a particular stereopair. This problem is more apparent towards the edge of any particular image in the pair and stereomatching processes can be very ineffective in such areas. Only a few matched points representing topographic high points are derived, and interpolation between isolated data points is very unreliable because topographic low points are not present. Accordingly, DoDs will always feature extensive and unrealistic elevation differences in these areas (see the example in Fig. 8). A precise reconstruction of these areas is beyond the scope of archival digital applications unless more images of the same date are available; hence a masking procedure was applied here. With the help of orthorectified images, hill-shaded representations, point clouds and DoDs, limits of rockwalls and forest boundaries were manually identified and excluded from the datasets.

CLIMATE FORCING AND GEOMORPHIC CHANGES IN ALPINE LANDSCAPES: AN ILLUSTRATION

Following the methodology presented above, a DEM has been generated for each available year from the 1960s to the present day. What this yields in terms of our

TABLE V. Limit of detection of change (LDC) with confidence limits of 68% and 90% computed using the error propagation methods explained in the text.

Year pair	*68% confidence limit (m)*	*90% confidence limit (m)*
2012–2005	1·100	1·804
2005–1999	1·296	2·126
1999–1995	1·118	1·833
1995–1988	0·990	1·623
1988–1983	1·135	1·862
1983–1977	1·244	2·040
1977–1967	1·121	1·839
2012–1988	0·793	1·300
1983–1967	1·208	1·981
2012–1967	0·894	1·466

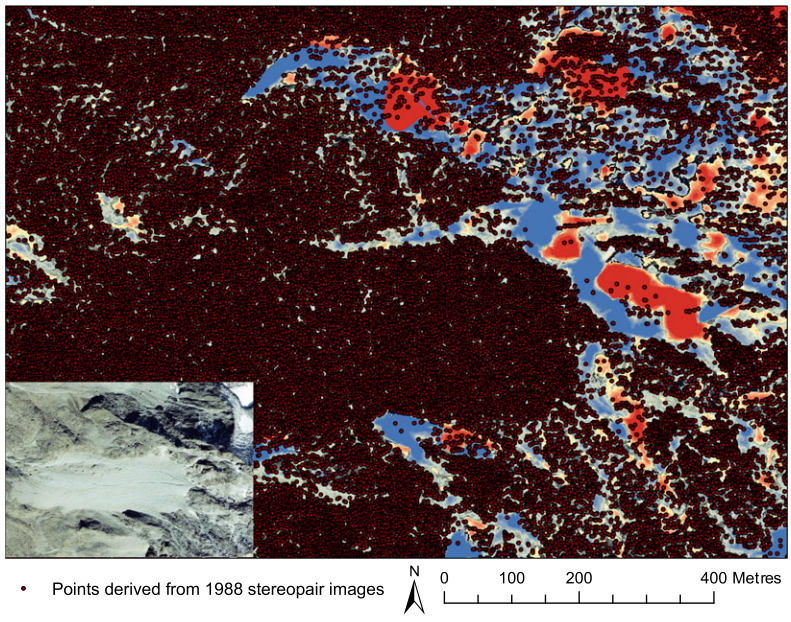

(a)

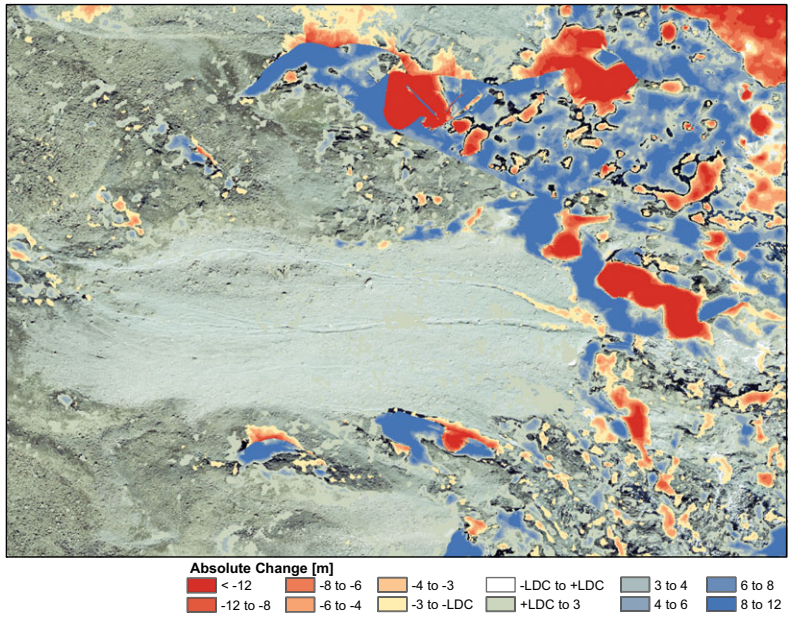

(b)

FIG. 8. (a) Ineffective stereomatching in rockwalls for a 1988 stereopair shown by data gaps. (b) Consequent unrealistic elevation changes featured in the 2012–1988 DoD (LDC = 1·30 m). Blues represent absolute changes greater than +6 m. Reds represent absolute changes greater than −8 m.

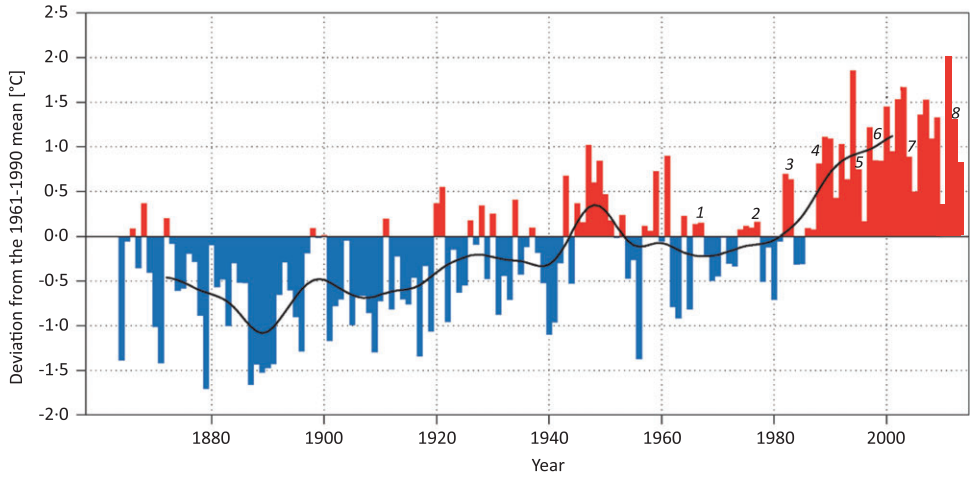

FIG. 9. Mean annual air temperatures in Switzerland between 1864 and 2013 as deviation from a reference mean established between 1961 and 1990. The black line indicates the 20-year weighted average (low-pass Gaussian filter). The numbers 1 to 8 indicate the year of available aerial imagery (see also Table I). Data from the Swiss Federal Office of Meteorology and Climatology (MeteoSwiss, 2014).

understanding of climate forcing in Alpine landscapes is now illustrated. Reference to the climatic conditions that affect the landscape is also necessary for this purpose; this is provided by the mean annual air temperature (MAAT) data for Switzerland (such measurements began in 1864 and are provided by the Swiss Federal Office of Meteorology and Climatology (MeteoSwiss, 2014)). Fig. 9 displays the deviation of each MAAT from a reference mean during the period 1961 to 1990. Such temperature data illustrate that the period 1967 to 1983 was a period of relative climate stability but from 1983 to 2012 relative climate warming occurred.

The interpretation of results is helped by a reference to the spatial assemblage of landforms present; a geomorphological map of the region provided by Lambiel et al. (2015) was used for this purpose (Fig. 10, right), allowing the identification of which components of the landscape are most sensitive to both climate cooling and climate warming. The comparison between 1983 to 1967 and 2012 to 1988 DoDs is presented in Fig. 10 (left and centre, where absolute changes and LDC have been normalised by year) and illustrates a distinct response to warming and stable periods. During the stable/cold period the landscape is also very stable, except for glaciers and debris-covered glacier systems that experience a noticeable gain in volume in their upper part; this can be explained by a process of cryogenesis (very low temperatures and their effects). On the other hand, the period from the mid-1980s to 2012 features enhanced hillslope activity, particularly in rock glaciers, rockslides and debris flow channels. It is apparent that warming climatic conditions caused extensive shrinking of glacial systems, especially in the accumulation area and the glacier front zone. Yet, ice ablation is compensated by cold-period ice supply in the central part of the Tsarmine glacier (northern areas in Fig. 10) and at the front of the Tsa glacier (south-east on the geomorphological map in Fig. 10). These changes aside, perhaps one of the most interesting elements of Fig. 10 is the relative stability of this landscape despite recent climate changes.

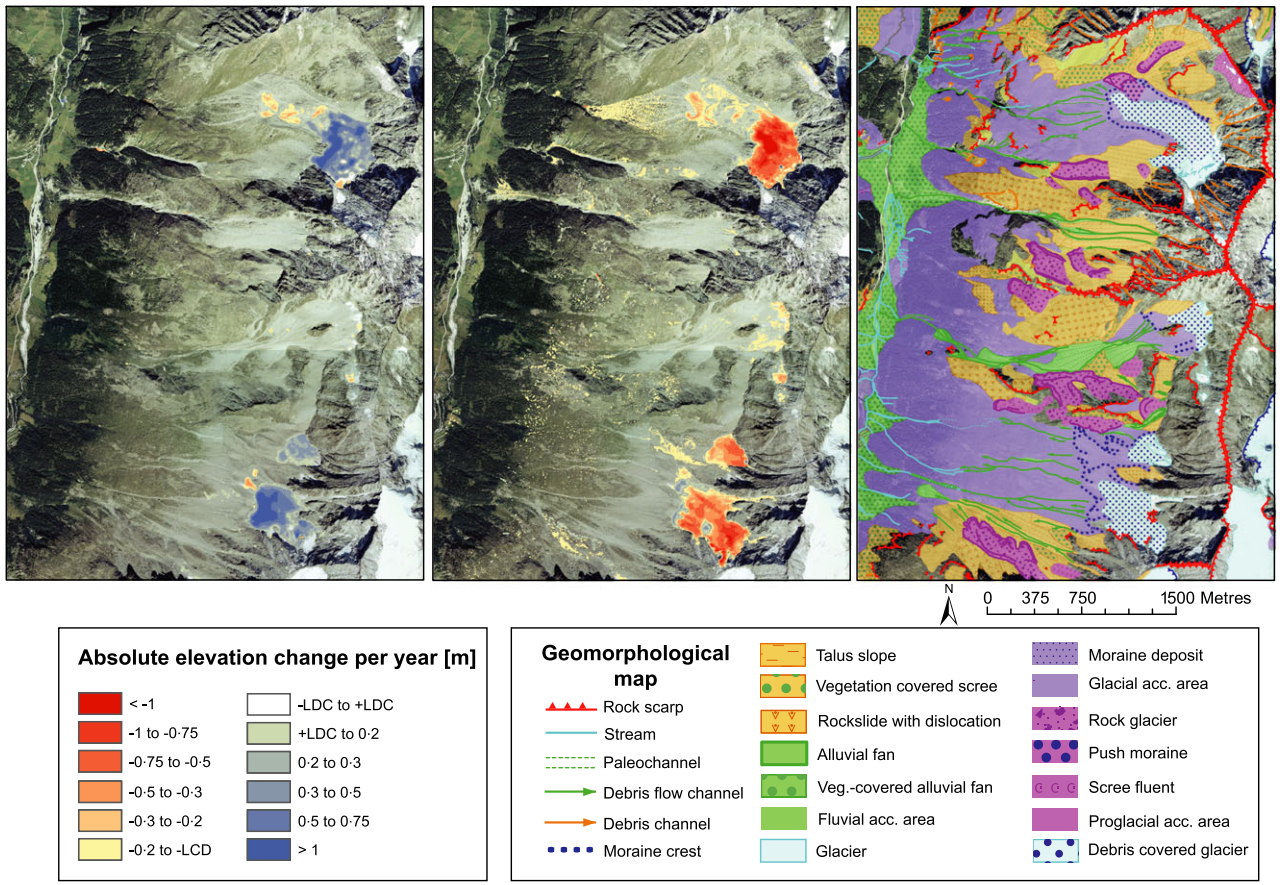

FIG. 10. DEMs of difference comparison between the cold period (left, 1983–1967, yearly LCD = 0·124 m) and warming period (centre, 2012–1988, yearly LDC = 0·054 m). The geomorphological map (right) acts as a reference to the underlying spatial assemblage of landforms present (Lambiel et al., 2015). A distinct landscape response to both the warming and cooling periods is found. The most evident examples include: cryogenesis in glacier accumulation areas versus glacier retreat and increase in activity of rock glaciers under warming conditions.

CONCLUSION

In the present research, a complete workflow for the application of archival aerial photogrammetry to quantify geomorphological changes and climate forcing of high mountain landscapes has been proposed. Archival aerial photogrammetry applications remain challenging in Alpine environments for various reasons, including wide elevation differences, suboptimal quality and varying scale of imagery, and the difficulties of establishing ground control. The approach articulated in this study and lessons learned are intended to help geomorphologists work with archival aerial imagery for other sites. Ways to overcome these challenges have been presented, including techniques to establish appropriate control, conducting careful analysis outcomes at every step and using a conservative approach for error propagation. Accordingly, this paper demonstrates that it is possible to employ archival imagery to obtain high-quality DEM data suitable for geomorphological research. Results are encouraging and suggest that, even for complex and steep topography, the information locked in archival aerial photogrammetry represents a valuable and exploitable resource. It should be stressed that this technique can only observe changes in elevation greater than 1 to 1·5 m when using imagery of the scale used here (approximately 1:20 000). This figure equates well with the expected height accuracy of ± 1 to ± 3 parts per 10 000 of the flying height at a single epoch, cited in previous work (Fryer et al., 1994). Erosion and deposition patterns that create a vertical signal smaller than this cannot be detected reliably using archival aerial imagery of this scale and historical quality.

ACKNOWLEDGEMENTS

This research was supported by the Herbette Foundation of the University of Lausanne, the Vaud Canton and the Valais Canton. The authors would like to thank the University of Fribourg for their collaboration and Christophe Lambiel for providing the geomorphological map used to improve data quality and to interpret the results.

REFERENCES

AGUILAR, F. J., AGÜERA, F., AGUILAR, M. A. and CARVAJAL, F., 2005. Effects of terrain morphology, sampling density, and interpolation methods on grid DEM accuracy. *Photogrammetric Engineering & Remote Sensing*, 71(7): 805–816.

ARUN, P. V., 2013. A comparative analysis of different DEM interpolation methods. *The Egyptian Journal of Remote Sensing and Space Science*, 16(2): 133–139.

BENNETT, G. L., MOLNAR, P., MCARDELL, B. W., SCHLUNEGGER, F. and BURLANDO, P., 2013. Patterns and controls of sediment production, transfer and yield in the Illgraben. *Geomorphology*, 188: 68–82.

CHANDLER, J. and COOPER, M., 1988. Monitoring the development of landslides using archival photography and analytical photogrammetry. *Land and Minerals Surveying*, 6(11): 576–584.

CHANDLER, J. H. and MOORE, R., 1989. Analytical photogrammetry: a method for monitoring slope instability. *Quarterly Journal of Engineering Geology*, 22(2): 97–110.

CHANDLER, J. H. and BRUNSDEN, D., 1995. Steady state behaviour of the Black Ven mudslide: the application of archival analytical photogrammetry to studies of landform change. *Earth Surface Processes and Landforms*, 20(3): 255–275.

COOPER, M. A. R., 1998. Datums, coordinates and differences. Chapter 2 in *Landform Monitoring, Modelling and Analysis* (Eds. S. N. Lane, K. S. Richards & J. H. Chandler). Wiley, Chichester, UK. 454 pages: 21–36.

DEWEZ, T. J. B., ROHMER, J., REGARD, V. and CNUDDE, C., 2013. Probabilistic coastal cliff collapse hazard from repeated terrestrial laser surveys: case study from Mesnil Val (Normandy, northern France). *Journal of Coastal Research, Special Issue*, 65: 702–707.

DISSART, O. and JAMET, O., 1995. 3D reconstruction of buildings from stereo-images using both monocular analysis and stereomatching: an assessment within the context of cartographic production. *Proceedings of the Society of Photo-Optical Instrument Engineers*, 2486: 255–266.

FISCHER, L., EISENBEISS, H., KÄÄB, A., HUGGEL, C. and HAEBERLI, W., 2011. Monitoring topographic changes in a periglacial high-mountain face using high-resolution DTMs, Monte Rosa East Face. *Italian Alps. Permafrost and Periglacial Processes*, 22(2): 140–152.

FONSTAD, M. A., DIETRICH, J. T., COURVILLE, B. C., JENSEN, J. L. and CARBONNEAU, P. E., 2013. Topographic structure from motion: a new development in photogrammetric measurement. *Earth Surface Processes and Landforms*, 38(4): 421–430.

FÖRSTNER, W., 1986. A feature-based correspondence algorithm for image matching. *International Archives of Photogrammetry and Remote Sensing*, 26(3/3): 150–166.

FRYER, J. G., CHANDLER, J. H. and COOPER, M. A. R., 1994. On the accuracy of heighting from aerial photographs and maps: implications to process modellers. *Earth Surface Processes and Landforms*, 19(6): 577–583.

GOOCH, M. J. and CHANDLER, J. H., 2001. Failure prediction in automatically generated digital elevation models. *Computers & Geosciences*, 27(8): 913–920.

HÖHLE, J. and HÖHLE, M., 2009. Accuracy assessment of digital elevation models by means of robust statistical methods. *ISPRS Journal of Photogrammetry and Remote Sensing*, 64(4): 398–406.

INTERGRAPH CORPORATION, 2014. *ERDAS IMAGINE Help*. Huntsville, Alabama, USA. http://www.hexagongeospatial.com [Accessed: 5th December 2014].

JAMES, M. R. and ROBSON, S., 2014. Mitigating systematic error in topographic models derived from UAV and ground-based image networks. *Earth Surface Processes and Landforms*, 39(10): 1413–1420.

KÄÄB, A. and VOLLMER, M., 2000. Surface geometry, thickness changes and flow fields on creeping mountain permafrost: automatic extraction by digital image analysis. *Permafrost and Periglacial Processes*, 11(4): 315–326.

KNEISEL, C. and KÄÄB, A., 2007. Mountain permafrost dynamics within a recently exposed glacier forefield inferred by a combined geomorphological, geophysical and photogrammetrical approach. *Earth Surface Processes and Landforms*, 32(12): 1797–1810.

KNIGHT, J. and HARRISON, S., 2013. The impacts of climate change on terrestrial Earth surface systems. *Nature Climate Change*, 3(1): 24–29.

LAMBIEL, C., MAILLARD, B., KUMMERT, M. and REYNARD, E., 2015. Geomorphological map of the Hérens Valley (Swiss Alps). *Journal of Maps*, DOI:10·1080/17445647·2014·999135.

LANE, S. N., CHANDLER, J. H. and RICHARDS, K. S., 1994. Developments in monitoring and modelling small-scale river bed topography. *Earth Surface Processes and Landforms*, 19(4): 349–368.

LANE, S. N., JAMES, T. D. and CROWELL, M. D., 2000. Application of digital photogrammetry to complex topography for geomorphological research. *Photogrammetric Record*, 16(95): 793–821.

LANE, S. N., WESTAWAY, R. M. and HICKS, D. M., 2003. Estimation of erosion and deposition volumes in a large, gravel-bed, braided river using synoptic remote sensing. *Earth Surface Processes and Landforms*, 28(3): 249–271.

LANE, S. N., REID, S. C., WESTAWAY, R. M. and HICKS, D. M., 2004. Remotely sensed topographic data for river channel research: the identification, explanation and management of error. Chapter 6 in *Spatial Modelling of the Terrestrial Environment* (Eds. R. E. J. Kelly, N. A. Drake & S. L. Barr). Wiley, Chichester, UK. 276 pages: 113–136.

LANE, S. N., WIDDISON, P. E., THOMAS, R. E., ASHWORTH, P. J., BEST, J. L., LUNT, I. A., SMITH, G. H. S. and SIMPSON, C. J., 2010. Quantification of braided river channel change using archival digital image analysis. *Earth Surface Processes and Landforms*, 35(8): 971–985.

LEICA GEOSYSTEMS GEOSPATIAL IMAGING, 2006. *Leica Photogrammetry Suite Automatic Terrain Extraction User's Guide*. Norcross, Georgia, USA. 154 pages.

METEOSWISS, 2014. *Climate Today: Trends in Switzerland*. http://www.meteoswiss.admin.ch/home/climate/present-day/climate-trends.html [Accessed: 1st December 2014].

MILLEDGE, D. G., LANE, S. N. and WARBURTON, J., 2009. The potential of digital filtering of generic topographic data for geomorphological research. *Earth Surface Processes and Landforms*, 34(1): 63–74.

REMONDINO, F., SPERA, M. G., NOCERINO, E., MENNA, F. and NEX, F., 2014. State of the art in high density image matching. *Photogrammetric Record*, 29(146): 144–166.

REYNARD, E., LAMBIEL, C. and LANE, S. N., 2012. Climate change and integrated analysis of mountain geomorphological systems. *Geographica Helvetica*, 67(1–2): 5–14.

SCHWAB, M., RIEKE-ZAPP, D., SCHNEIDER, H., LINIGER, M. and SCHLUNEGGER, F., 2008. Landsliding and sediment flux in the Central Swiss Alps: a case study from the Schimbrig landslide. *Entlebuch. Geomorphology*, 97(3–4): 392–406.

SMALL, R. J., BEECROFT, I. R. and STIRLING, D. M., 1984. Rates of deposition on lateral moraine embankments, Glacier de Tsidjoure Nouve, Valais. *Switzerland. Journal of Glaciology*, 30(106): 275–281.

TAYLOR, J. R., 1997. *An Introduction to Error Analysis: The Study of Uncertainties in Physical Measurements*. Second edition. University Science Books, Sausalito, California, USA. 327 pages.
WALSTRA, J., DIXON, N. and CHANDLER, J. H., 2007. Historical aerial photographs for landslide assessment: two case histories. *Quarterly Journal of Engineering Geology and Hydrogeology*, 40(4): 315–332.
WELCH, R. and JORDAN, T. R., 1983. Analytical non-metric close-range photogrammetry for monitoring stream channel erosion. *Photogrammetric Engineering & Remote Sensing*, 49(3): 367–374.
WICKENS, E. and BARTON, N. R., 1971. The application of photogrammetry to the stability of excavated rock slopes. *Photogrammetric Record*, 7(37): 46–54.

Résumé

Les changements climatiques récents et à venir peuvent conduire à des changements dans la morphologie des paysages. Cependant, ces modifications sont susceptibles d'avoir une distribution très étendue ce qui rend difficile leur mesure directe localement, et ces mesures ne sont généralement pas disponibles à des cadences décennales. Des images aériennes ont pourtant été acquises par de nombreuses agences nationales depuis les années 1950 et des archives importantes subsistent. Ils est important de libérer les informations provenant de ces sources de données, car leur échelle de temps permet de vérifier des hypothèses non confirmées concernant l'impact d'un changement climatique rapide sur les environnements alpins. Cependant, des applications photogrammétriques de cet type sont confrontées à la complexité de la topographie (notamment les occlusions et les grandes dénivellations) et aux variations de la texture des images. Une chaîne complète de traitement est décrite, depuis les données brutes jusqu'à l'interprétation des résultats. Elle est appliquée à des images de Val d'Héréns, en Suisse, un paysage contenant un ensemble de reliefs glaciaires, périglaciaires, collinaires et fluviaux à des altitudes de 1800 à 3600 m, depuis les années 1960 à nos jours. Ces changements révèlent des caractéristiques importantes de l'érosion et de la sédimentation sur l'ensemble du paysage, à l'échelle de la décennie.

Zusammenfassung

Aktuelle und zukünftige Klimaänderungen können Einfluss auf Änderungen der Landschaft in geomorphologischen Prozessen und deren Zyklen haben. Allerdings sind solche Änderungen oft weit verstreut, was eine lokale Messung erschwert und es gibt praktisch keine Messungen mit einem Intervall von einer Dekade und mehr. Allerdings gibt es in vielen Ländern Archive von Luftbildern seit ca. 1950. Aus diesen Datenquellen können wichtige Informationen zur Änderung einer Landschaft extrahiert werden. Der abgedeckte Zeitraum erlaubt es u.U. bis jetzt unentdeckte Hypothesen zum Einfluss von schnellen Klimaänderungen im Alpenraum abzuleiten. Allerdings ist die Anwendung der Photogrammetrie eine Herausforderung durch die topographische Komplexität (inklusive Verdeckungen und extremen Höhenunterschieden) und der Variationen in der Bildtextur. Dieser Beitrag umfasst eine komplette Beschreibung des Arbeitsflusses von den Rohdaten zur Ableitung und Interpretation der Ergebnisse. Als Testdaten dienen Bilddaten des Val d'Héréns, Schweiz, einer Landschaft mit einer Ansammlung von glazialen und periglazialen Landformen, sowie Berghängen und Flusslandschaften über einen Höhenbereich von 1800 bis 3600 m von den 1960er Jahren bis heute. Die beobachteten Änderungen ergeben Hinweise auf wichtige Eigenschaften von Erosionen und Ablagerungen der Landschaft über Jahrzehnte hinweg.

Resumen

El reciente y futuro cambio climático puede conducir a cambios en el paisaje en procesos geomorfológicos y las tasas de proceso. Sin embargo, estas modificaciones son susceptibles de ser ampliamente distribuidas, por lo que su medición directa es difícil y casi no existen tales mediciones a intervalos de

décadas. Sin embargo, muchas agencias nacionales desde la década de 1950 han ido adquiriendo imágenes aéreas y existiendo importantes archivos. Desbloquear el acceso a estas fuentes de datos es importante porque su escala temporal permitirá documentar importantes hipótesis sin resolver en relación con el impacto del rápido cambio climático en entornos alpinos. Sin embargo, este tipo de aplicaciones fotogramétricas son un desafío a causa de la complejidad topográfica (incluyendo las oclusiones y grandes rangos de elevación) y las variaciones en textura de la imagen. Se describe una metodología completa de trabajo a partir de datos en bruto para el tratamiento y la interpretación de los resultados. Se ha aplicado a las imágenes de Val d'Héréns, Suiza, un paisaje que contiene un conjunto de glaciar, periglaciar, laderas y geoformas fluviales en un rango de alturas de 1800 a 3600 m desde la década de 1960 hasta la actualidad. Revelándose cambios importantes en las características de erosión del paisaje y deposición de residuos a lo largo de las décadas.

摘要

最近和未来的气候变化可能导致的地貌以及地貌变迁过程中的景观变化。然而,这样的变化分布广泛,且其时间尺度可能是*10*年,因此直接测量该变化非常困难。然而,许多国家从上世纪*50*年代开始获取航空影像,作为档案保存。从这些数据源中挖掘信息是重要的,因为该尺度的景观变化可能可以提取重大的悬而未决的假设,尤其针对高山地快速的气候变化。但是,这样的摄影测量应用是具有挑战性的,主要原因是地形非常复杂且图像纹理变化。本文提出并描述了一个完整的从原始数据处理到结果描述的工作流。该工作流能够应用到瑞士*Val d'Héréns* 谷地区从 *60* 年底到现在的影像,地貌包含冰川,冰缘组合,山坡和河流,其高程范围变化从 *1800*到*3600 m*,这些变化揭示在*10*年尺度上景观变化中侵蚀和沉积的重要特征。